BUBBLE GENERATION IN A FLOWING LIQUID MEDIUM AND RESULTING TWO-PHASE FLOW IN MICROGRAVITY

S. C. Pais[1], Y. Kamotani[2], A. Bhunia[3] and S. Ostrach[4], [1,2,3,4] Department of Mechanical & Aerospace Engineering, Glennan Building, Case Western Reserve University, 10900 Euclid Avenue, Cleveland, OH 44106, [2] Corresponding Author, e-mail: yxk@po.cwru.edu,

INTRODUCTION

The development of two-phase flow research under reduced and microgravity conditions is prompted by a wide range of space applications, such as, thermal energy and power generation, propulsion, cryogenic storage and long duration life support systems; necessary for programs, such as NASA's Human Exploration for the Development of Space (HEDS). Study of gas-liquid flows in reduced gravity is important for the design of two-phase thermal control systems, intended to replace conventional pumped liquid loops[1, 2]. The main advantage of a two-phase thermal control system is its reduced weight, which is of utmost importance since any weight saving for payload transfer to orbit signifies lower launch costs.

Under normal gravity conditions, when gas is injected through an orifice into a quiescent liquid medium, the bubble grows and detaches quite readily due to the buoyancy force. Under reduced gravity conditions, the detaching role of the buoyancy force is significantly diminished, giving rise to uncontrollably larger bubbles than those obtained in normal gravity. Consequently, another bubble detaching force is required in order to control bubble size and frequency of formation. A practical solution is to use flowing liquid and utilize its drag force for bubble detachment[3,4].

Two configurations generally considered for bubble dispersion in a flowing liquid are the co-flow and the cross-flow geometry. In the co-flow configuration, the dispersed phase is introduced through a nozzle in the same direction with the liquid flow; whereas in the cross-flow geometry, gas is injected perpendicular to the direction of liquid flow. Of the three major two-phase flow patterns, namely bubble, slug and annular[5], only bubble and annular flows are used in space based systems[6]. In this work, we are concentrating on the bubbly flow regime.

For normal[7, 8] and reduced gravity[9, 10], bubble generation in a quiescent liquid has been extensively studied. Reduced gravity bubble formation in the cross-flow configuration has been recently reported by several investigators[4, 11, 12]. On the other hand, the co-flow configuration has only been considered in normal gravity in order to observe the effect of liquid velocity on bubble detachment[12, 13]. Under reduced gravity conditions bubble generation and resulting two-phase flow by multiple nozzle injection along the periphery of the flow conduit has been reported by several investigators[5,6]. With multiple nozzle injection, due to unpredictable coalescence of adjacent bubbles, it is difficult to control accurately the void fraction of the ensuing two-phase flow. A better alternative is controlled bubble generation via single nozzle injection.

In this work, we investigate bubble generation by gas injection via a single nozzle in a co- and cross-flow system. Experiments using air and water are performed in parabolic flight aboard the modified DC-9 Reduced Gravity Research Aircraft at NASA Lewis Research Center. Effects of surrounding liquid velocity and two-phase flow conduit geometry on the bubble diameter and the associated void fraction are investigated. For the co-flow geometry, we have also developed a theoretical model, based on an overall balance of forces acting on the bubble. Predictions of bubble diameter and formation frequency using the present model show good agreement with our experimental results.

EXPERIMENTAL STUDY

In reduced gravity, the bubble diameter (D_B) is dependent on fluid properties, flow geometry and flow conditions.

$$D_B = f (Q_d, Q_c, D_P, D_N, \sigma, \mu_c, \mu_d, \rho_c, \rho_d)$$

where Q_d is the volumetric gas flow rate, Q_c is the volumetric liquid flow rate, D_P is the pipe diameter, D_N is the nozzle diameter, σ is the surface tension, μ_c and ρ_c are the dynamic viscosity and density of the liquid phase, while μ_d and ρ_d are the dynamic viscosity and density of the gas phase. In this study, we are investigating the effect of flow conditions (Q_d, Q_c) and flow geometry (D_P, D_N) on bubble diameter (D_B).

Apparatus and Methods

Our experiments are conducted aboard the modified DC-9 Reduced Gravity Research Aircraft which provides the investigator with 20 seconds of 0.01 g reduced gravity environment. Out of this time period an estimated 15 seconds is allotted for acquisition of experimental data. The reproducibility of data between two consecutive trajectories is within ± 5%. The present two-phase flow experiments are performed with an air-water system using three different sets of pipe diameters (D_p = 1.27 cm, 1.9 cm and 2.54 cm). In addition, two different ratios of nozzle to pipe diameters are considered ($D_n^* = D_n/D_p$ = 0.1 and 0.2). Depending on the two-phase flow pipe diameter, superficial gas (U_{GS} = $4Q_d/\pi D_p^2$) and liquid velocities (U_{LS} = $4Q_c/\pi D_p^2$) are varied from 8 to 70 cm/s. In general, for each data point acquired, two dive trajectories are executed.

The co-flow test section (figure 1) consists of a Plexiglas pipe, which acts as the two-phase flow conduit.
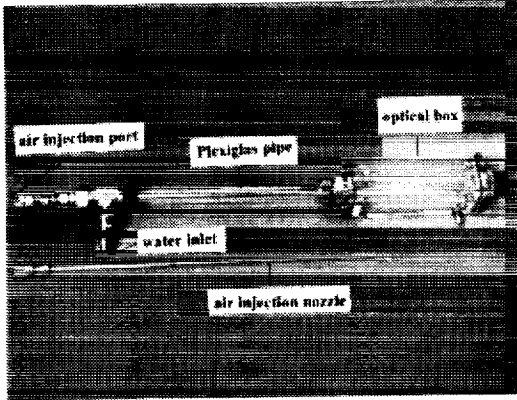
70

Fig 1: Co-flow experimental test section

A tee branch fitting is mounted on the inlet side of the pipe. Dry and filtered air is injected through a stainless steel tube, which acts as the gas injection nozzle and protrudes into the pipe. Distilled water is introduced through the remaining port of the tee branch fitting. The water and air mixing region is surrounded by a Plexiglas visual rectangular box filled with water, which eliminates optical distortion of the generated bubble.

The cross flow test section, shown in figure 2, is machined as a tee section from a rectangular piece of Plexiglas stock. Two orthogonally positioned, equal diameter holes are bored into the Plexiglas tee, one merging into the other. Through one of these holes, air is injected via a stainless steel tube. The other hole acts as the water inlet tube as well as the two-phase flow conduit.
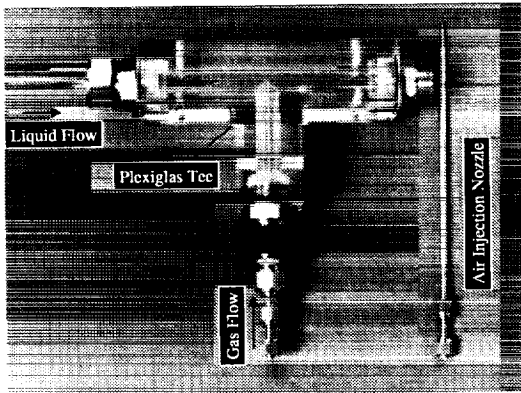

Fig 2: Cross-flow experimental test section

The complete experimental test section assembly is integrated within the Learjet Two-phase Flow Apparatus, developed and described by McQuillen and Neumann[14]. The bubble generation process is recorded with a high speed video camcorder (250 frames/sec). For every experimental run, a new batch of distilled water is used to minimize contamination at the bubble surface.

Experimental bubble diameter is obtained from the flight experiment video by using THIN 2.0^e and OPTIMAS 5.1^e image acquisition and processing software packages. The geometrically averaged bubble diameter for each of three consecutively detached bubbles in the vicinity of the gas injection nozzle is first calculated. The bubble diameter reported in this work is the arithmetic average of these three values. The standard deviation for bubble diameter measurement is within $\pm 2.5\%$ of the mean diameter value. Uncertainty errors in flow velocity measurement have an upper limit of $\pm 5\%$ of the obtained value. A more elaborate discussion on experimental procedure and data acquisition is given by Pais[15].

Co-flow Configuration Results

The important role played by the flowing liquid on bubble detachment in reduced gravity is shown in figure 3. Experimental data presented in this figure is obtained for a fixed pipe diameter of 1.9 cm and a gas flow rate of 51 cm^3/s (cc/s). Two sets of nozzle diameters ($D_N = 0.19$ cm and 0.38 cm) are used. For both nozzle diameters, as superficial liquid velocity is increased, the bubble diameter decreases. The drag induced by the surrounding liquid flow results in faster detachment of the bubble, thereby decreasing its size. It is further observed that bubble diameter increases with nozzle diameter, which can be explained from the fact that with a larger injection nozzle more gas is fed into the bubble.
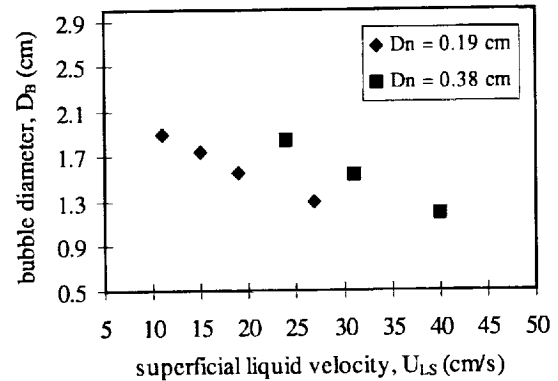

Fig 3: Effect of nozzle diameter and superficial liquid velocity on bubble diameter. Fixed $Q_d = 51$ cc/s and $D_P = 1.9$ cm.

Variation of bubble size with increasing volumetric gas flow rate and pipe diameter is displayed in figure 4. The volumetric liquid flow rate and the nozzle diameter are kept constant at $Q_c = 40$ cc/s and $D_N = 0.19$ cm. Experiments are conducted with three different pipe diameters, $D_P = 1.27$, 1.9 and 2.54 cm by varying the gas flow rate from 16 to 40 cc/s. It is obvious that bubble diameter increases with increasing gas flux and pipe diameter. At a fixed Q_c, an increase in pipe diameter implies a reduction in co-flowing liquid velocity and therefore liquid drag. Larger bubbles are
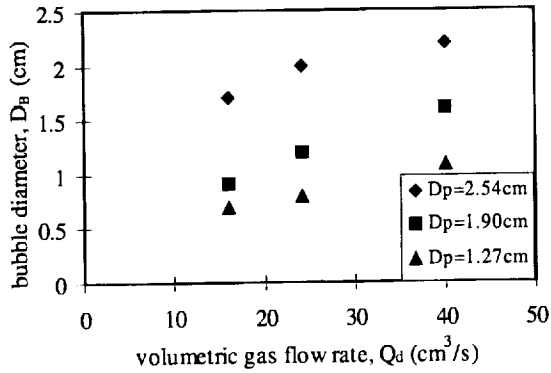
formed when drag induced by the flowing liquid is reduced.

Fig 4: Variation of bubble diameter with volumetric gas flow rate and flow conduit diameter. Fixed Q_c = 40 cc/s and D_N = 0.19 cm.

Figure 5 displays variation of void fraction (V_f) with volumetric gas and liquid flow rates. Void fraction is defined as the ratio of volume occupied by the gas phase to total volume of fluid within a given section of the two phase flow conduit. Mathematically, for a single bubble in the bubbly flow regime, this relationship can be written as $V_f = 2D_B^3/3D_P^2\Delta$, where Δ is the distance between the front of the detached bubble and the front of the previously detached bubble. In the bubbly flow regime the maximum value of the void fraction is 2/3 ($D_B = D_P$), beyond which formation of Taylor bubbles (slugs) occurs. In the slug flow regime, void fraction can exceed the value of 2/3, its upper limit being 1.
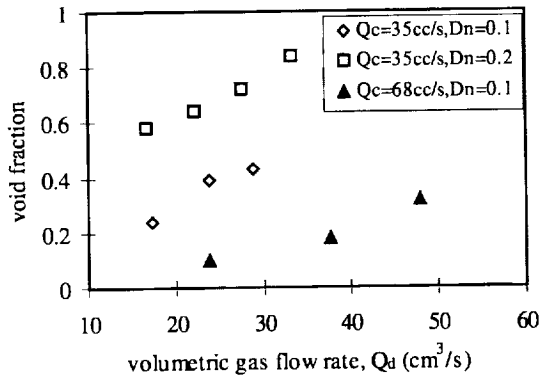

Fig 5: Dependence of void fraction on gas and liquid flow rate with respect to variation in nozzle diameter. D_P is fixed at 1.9 cm.

Void fraction, which is directly proportional to the bubble diameter, increases with gas flow rate and nozzle diameter, while decreasing with liquid flow rate. For the data presented in this graph, the pipe diameter is fixed at 1.9 cm. It is observed that at $D_N{}^*$ = 0.1 (D_N = 0.19 cm), for two different liquid flow rates, Q_c = 35 and 68 cc/s, the void fraction is less than 2/3, indicating occurrence of the bubbly flow regime. On the other

hand, for Q_c = 35 cc/s and $D_N{}^*$ = 0.2 (D_N = 0.38 cm), the void fraction exceeds the value of 2/3 for Q_d = 29 and 33 cc/s, suggesting formation of Taylor bubbles at such flow conditions.

Cross Flow Configuration Results

In the cross-flow configuration, bubble diameter as a function of superficial liquid velocity and nozzle diameter is shown in figure 6. This plot displays data taken with the 1.27 diameter test section at a constant gas flow rate of 44 cc/s. For two different nozzle diameters (D_N = 0.127 and 0.254 cm), the superficial liquid velocity (U_{LS}) is varied from 20 to 60 cm/s. It is observed that the bubble diameter decreases with increasing superficial liquid velocity for a given gas injection geometry at a constant gas flow rate. Furthermore, it is noted that the bubble diameter increases with increasing nozzle diameter. The trends are similar to those displayed by the co-flow configuration.
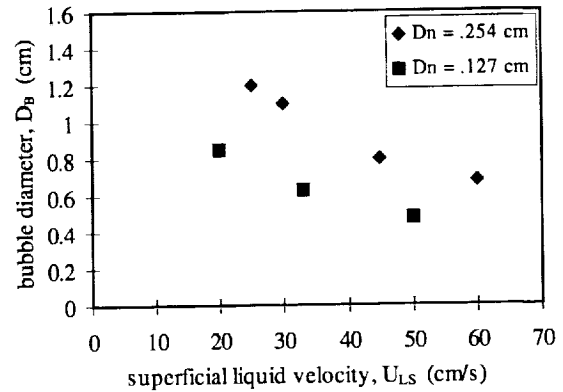

Fig 6: Effect of superficial liquid velocity and nozzle diameter on bubble size for a fixed Q_d = 44 cm³/s and D_P = 1.27 cm.
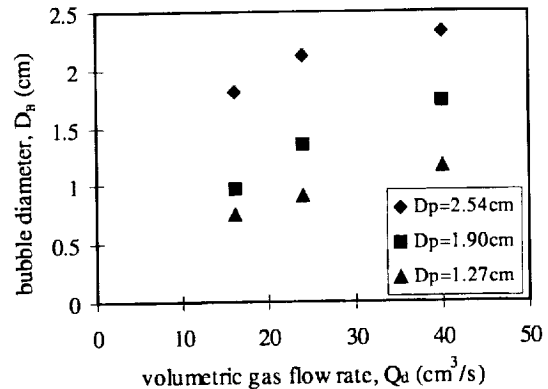

Fig 7: Variation of bubble diameter with respect to gas flow rate and pipe diameter at a fixed Q_c = 40 cm³/s and D_N = 0.19 cm.

Figure 7 shows the variation of bubble diameter with volumetric gas flow rate and pipe diameter at a constant liquid flow rate of 40 cc/s. For acquiring this data, three distinct volumetric gas flow rates are used, namely 16, 24 and 40 cc/s. Experiments are performed

using the 1.27, 1.9 and 2.54 cm diameter test sections, keeping the nozzle diameter constant at 0.19 cm. Note that bubble size grows with increasing gas flow rate and pipe diameter at a constant liquid flow rate. Figure 4 and figure 7 display bubble diameters at identical flow geometry and conditions for co and cross flow configurations. It is interesting to observe that at similar flow conditions and geometry, somewhat larger bubbles are generated by using the cross-flow configuration rather than the co-flow configuration.

A plot of void fraction (V_f) values as a function of volumetric gas and liquid flow rates is presented in figure 8. This experimental data is obtained using the 1.9 cm diameter test section for two different nozzle diameters, $D_N = 0.19$ and 0.38 cm. For two different liquid flow conditions ($Q_c = 51$ and 68 cc/s), the gas flow rate is varied from 16 to 49 cc/s. In the cross-flow configuration, analogous to the co-flow geometry, the void fraction increases with increasing gas flow rate and decreases with increasing surrounding liquid flow. Furthermore, it is observed that V_f increases with gas injection nozzle diameter.
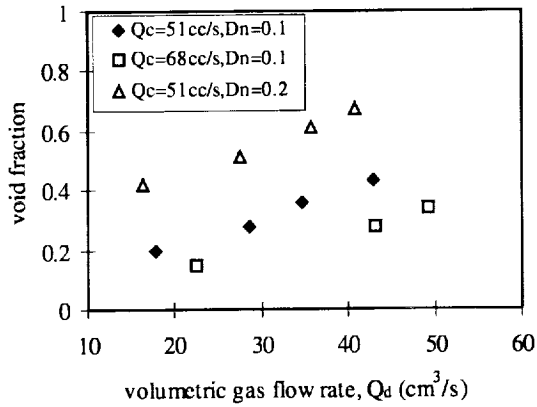

Fig. 8: Effect of volumetric gas and liquid flow rates on void fraction with respect to variation in nozzle diameter for constant pipe diameter of 1.9 cm.

Comparison of Co- and Cross-flow Configuration

Bubble diameters and void fraction obtained using the co-flow system are compared with corresponding values obtained in the cross-flow geometry. The data displayed in figure 9, is obtained using a 1.9 cm diameter test section at constant liquid flow rate of 68 cc/s with a 0.38 cm nozzle diameter. The volumetric gas flow rate is varied from 21 to 70 cc/s. It is observed that at similar values of gas and liquid flow rates as well as similar nozzle and pipe diameters, bubbles generated by using the cross-flow configuration are slightly larger in size relative to those obtained in co-flow geometry. Therefore, the void fraction of the resulting two-phase flow also follows a similar trend.
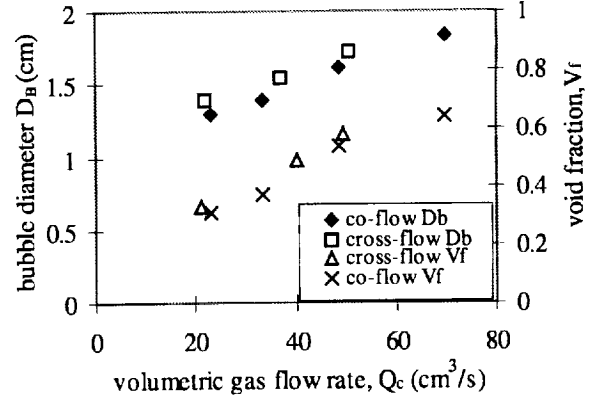

Fig 9: Comparison of bubble diameter and void fraction for co and cross-flow configuration. Fixed $Q_c = 68$ cc/s, $D_P = 1.9$ cm and $D_N = 0.38$ cm.

THEORETICAL STUDY

In parallel to the experimental work, we have developed a theoretical model to describe the bubble detachment process from which we obtain the detached bubble diameter and formation time in a co-flow configuration, as shown in figure 10.
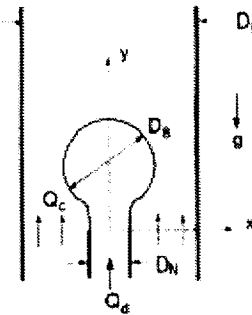

Fig. 10: Schematic of co-flow configuration.

The current model, which is valid for both normal and reduced gravity conditions at constant gas flux, is employed to investigate single bubble generation in the dynamic ($Q_d = 1 - 1000$ cc/s) and bubbly flow regime ($D_B < D_P$). The focus of the model is to identify the important forces involved in the process of bubble formation and their role on bubble detachment. The bubble shape is assumed spherical throughout the formation process. Hence, for constant flow conditions, the rate of change of bubble volume (V_B) is given as d V_B/d t $= Q_d =$ constant. Various important forces involved in the bubble generation process are:

$$F_B = V_B (\rho_c - \rho_d) g$$

$$F_\sigma = \pi D_N \sigma$$

$$F_M = \rho_d \frac{Q_d^2}{(\pi/4) D_N^2}$$

$$F_D = S_D C_{DW} \frac{1}{2} \rho_c U_{eff}^2 A_{eff}$$

$$F_I = \frac{d}{dt} \left[\rho_d V_B \frac{ds}{dt} + \rho_c C_{MC} V_B U_{eff} \right]$$

where F_B, F_σ, F_M, F_D, F_I are respectively the buoyancy, surface tension, momentum flux, drag and inertia forces acting on the bubble. C_{DW} is drag coefficient of the bubble in presence of confining pipe walls; ds/dt is velocity of the bubble center away from the nozzle tip; U_{eff} is the relative velocity of bubble center w. r. t. superficial liquid velocity (U_{eff} = ds/dt – U_{LS}), A_{eff} is the effective area of the bubble on which the drag force acts; S_D is +1 or –1 for $U_{eff} < 0$ and $U_{eff} > 0$ respectively and C_{MC} is the added mass coefficient. Expressions for C_{MC}, C_{DW}, A_{eff} are given in our previous work[16].

Buoyancy and gas momentum flux always promote bubble detachment, while surface tension tries to prevent it. The inertia force has two components. Bubble inertia represented by the first term of the inertia force expression is always an attaching force. On the other hand, liquid inertia, represented by the second term, as well as the liquid drag can be either attaching or detaching, depending on whether $U_{eff} > 0$ or $U_{eff} < 0$.

Bubble generation occurs in two stages. During the first stage, defined as the expansion stage, the bubble grows radially due to incoming gas flux, however the bubble base remains attached to the nozzle. Bubble volume and growth rate during the expansion stage are respectively written as $V_B = (\pi/6) D_B^3(t)$ and ds/dt = ½ $dD_B(t)/dt$. A balance of the attaching and detaching forces marks the end of expansion stage ($D_B = D_{Be}$) and the beginning of the second stage, namely the detachment stage. During the detachment stage, the bubble continues to grow in size, the bubble volume being $V_B = (\pi/6) D_{Be}^3 + Q_d t$. The bubble moves away from the nozzle, but still remains attached to it via a neck region. The bubble center located at a distance Y from the nozzle tip, moves at a velocity d s/dt = d Y/d t. Bubble motion during the two stages is described by a balance of forces acting on it:

$$F_B + F_\sigma + F_M + F_D + F_I = 0$$

At the end of the detachment stage, the bubble departs the nozzle base due to neck pinch-off. The neck pinches off when its length becomes equal to the nozzle diameter. Therefore, the detachment criterion is written as:

$$L_N = Y - ½ D_B \geq D_N$$

Solving the force balance equations at the two stages of bubble formation, subject to the detachment criterion leads to a non-dimensional functional expression for the detached bubble diameter:

$$D_B^* = f(Re_P, We_P, Fr_P, U_{GS}^*, D_N^*, \rho^*)$$

Various dimensionless parameters are Reynolds number $Re_P = \rho_c U_{LS} D_P/\mu_c$; Weber number $We_P = \rho_c U_{LS}^2 D_P/\sigma$; Froude number $Fr_P = \rho_c U_{LS}^2/(\rho_c - \rho_d)g D_P$; Dimensionless superficial gas velocity $U_{GS}^* = U_{GS}/U_{LS}$; Dimensionless nozzle diameter $D_N^* = D_N/D_P$ and density ratio $\rho^* = \rho_d/\rho_c$. Further details on the method of solution and predictions resulting from this theoretical model are discussed by Bhunia et. al.[16].

A comparison of the present reduced gravity experimental data with predictions of the numerical model is shown in figure 11. This figure displays variation of dimensionless bubble diameter with respect to non-dimensional superficial gas velocity. Two different sets of dimensionless nozzle diameter (D_N^*) and for each D_N^* two different Reynolds number conditions are considered. The numerical predictions show good agreement with the experimental data. Over a wide range of Re_P, the present computational model predicts bubble diameter within ±10% of the experimental results.
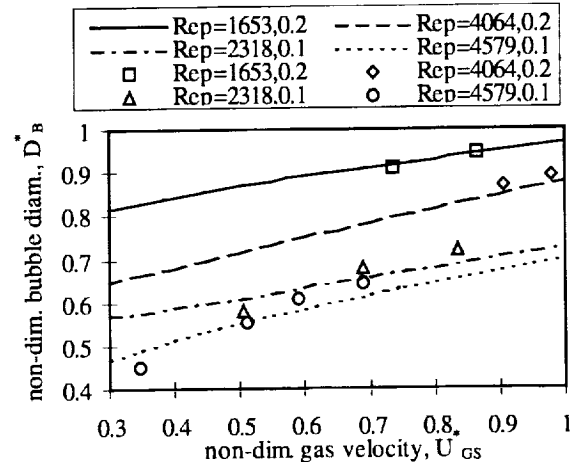

Fig. 11: Comparison of numerical predictions with experimental results. Solid and dotted line – Numerical predictions, symbols – experimental data.
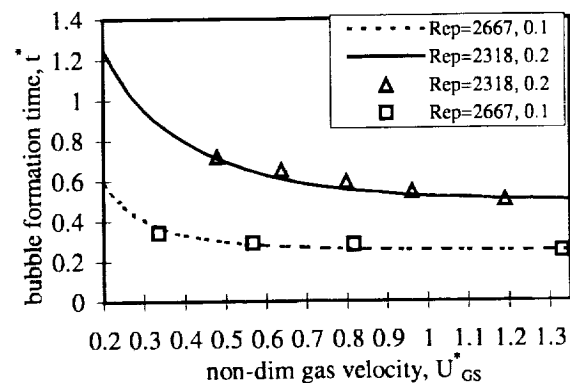

Fig 12: Comparison of computed dimensionless bubble formation time with reduced gravity experimental data. Solid and dotted line – numerical predictions, Symbols - experimental data; $D_N^* = 0.1$, $Re_P = 2667$, $We_P = 3.8$, $Fr_P = 4.4$; $D_N^* = 0.2$, $Re_P = 2318$, $We_P = 3.9$, $Fr_P = 8.0$.

The theoretical model is further validated by a comparison of the dimensionless bubble formation time ($t^* = t U_{LS}/D_P$) obtained from the model and the experimental data shown in figure 12. At low values of U_{GS}^*, the bubble formation time decreases sharply with increasing U_{GS}^*, until it reaches an asymptotic limit of constant time, irrespective of the U_{GS}^* value. It is fur-

74

ther observed that with increasing nozzle diameter when bubble size increases, it takes longer for the bubble to detach.

At higher superficial liquid velocity, the bubble deviates from its spherical shape, as assumed in this model. The present model agrees well with the experimental data up to a maximum Weber number of 30, which corresponds to a Reynolds number of 7500 for an air-water system using a 2.54 cm diameter pipe.

CONCLUSIONS

The present work focuses on bubble generation via single nozzle injection in a co- and cross-flowing liquid. This study is based on empirical data, obtained by performing experiments aboard the DC-9 Reduced Gravity Research Aircraft in parabolic flight. Effect of the flow conditions and geometry on detached bubble diameter and thereby void fraction of the resulting two-phase flow is investigated. It is shown that bubble diameter and void fraction increase with volumetric gas flow rate, pipe diameter and nozzle diameter, while they decrease with surrounding liquid flow. The important role of the continuous liquid flow in detaching bubbles under reduced gravity conditions is thus emphasized.

It is of interest to note that bubble size and corresponding void fraction are somewhat smaller for the co-flow system than for the cross-flow configuration at similar flow conditions and flow geometry. From empirical evidence it is shown that the void fraction can be readily controlled in case of single nozzle gas injection by varying the flow geometry or the flow conditions.

A theoretical model based on an overall force balance acting on the bubble during the two stages of generation is also developed. Two sets of forces, one aiding and other inhibiting bubble detachment are identified. The theoretical model predicts bubble diameter in good agreement with the reduced gravity experiments.

REFERENCES

[1]. S. Ostrach, Industrial Processes Influenced by Gravity, NASA CR-182140, C-21066-G, 1988.

[2]. S. Banerjee, Space Applications, Multiphase Flow and Heat Transfer: Bases and Application Workshop Santa Barbara, Calif., 1989.

[3]. S. C. Chuang and V. W. Goldschmidt, Bubble formation due to a Submerged Capillary Tube in Quiescent and Co-flowing Systems, J. Basic Eng., 92, 1970.

[4]. I. Kim, Y. Kamotani and S. Ostrach, Modeling Bubble and Drop Formation in Flowing Liquids in Microgravity, AIChE Journal, 40, 1, 1994.

[5]. C. Colin, J. Fabre and J. B. McQuillen, Bubble and Slug Flow in Microgravity Conditions-I , Dispersed Bubble and Slug Flow, Int. J. Multiphase Flow, 17, 4, 1991.

[6]. A. E. Dukler, J. Fabre, J. B. McQuillen and R. Vernon, Gas liquid Flow at Microgravity Conditions: Flow Patterns and Their Transitions, Int. J. Multiphase Flow, 14, 4, 1988.

[7]. N. Rabiger and A. Vogelpohl, Bubble Formation and its Movement in Newtonian and Non-Newtonian Liquids, in Encyclopedia of Fluid Mechanics, 3, Gulf Pub. Houston, 1986.

[8]. H. Tsuge, Hydrodynamics of Bubble Formation from Submerged Orifices, in Encyclopedia of Fluid Mechanics, 3, Gulf Pub. Houston, 1986.

[9]. O. Pamperin and H. Rath, Influence of Buoyancy on Bubble Formation at Submerged Orifice, Chem. Eng. Sci., 50, 19, 1995.

[10]. H. Merte, Jr., H. S. Lee and R. B. Keller, Report on Pool Boiling Experiment Flown on STS-47 (PBE-IA), STS-57 (PBE-IB) and STS-60 (PBE-IC), NASA CR-198465, 1996.

[11]. H. Nahra and Y. Kamotani, Bubble Formation and Detachment in Liquid Flow Under Normal and Reduced Gravity, 36th Aerospace Sciences Meeting & Exhibit, Reno, January, 1998.

[12]. H. N. Oguz, S. Takagi and M. Misawa, Production of Gas Bubbles in Reduced Gravity Environments, 3rd μg Fluid Phys. Conf, NASA Conf. Pub.-3338, 1996.

[13]. E. Sada, A. Yasunishi, S. Katoh and M. Nishioka, Bubble Formation in Flowing Liquid, Can. J. Chem. Eng., 56, 1978.

[14]. J. B. McQuillen and E. S. Neumann, Learjet Two Phase Flow Apparatus, NASA TM 106814, NASA LeRC, 1995.

[15]. S. C. Pais, Bubble Generation in a Continuous Liquid Flow Under Reduced Gravity Conditions, Ph. D Thesis, Case Western Reserve University, 1998.

[16]. A. Bhunia, S. C. Pais, Y. Kamotani and I. Kim, Bubble Formation in a Co-flow Configuration in Normal and Reduced Gravity, Accepted for publication in AIChE Journal.

ACKNOWLEDGEMENT